Light Scattering and Small-Angle Neutron Scattering Studies of Structures in a Semidilute Polymer Solution Induced under Oscillatory Shear Flow

Shin Saito,[†] Satoshi Koizumi,[†,§] Katsuo Matsuzaka,[†,‡] Shoji Suehiro,[†] and Takeji Hashimoto*[,†]

Department of Polymer Chemistry, Graduate School of Engineering, Kyoto University, Kyoto 606-8501, Japan and Advanced Research Center, Japan Atomic Energy Research Institute, Tokai-mura, Ibaraki-ken 319−1195, Japan

Received June 28, 1999; Revised Manuscript Received January 10, 2000

ABSTRACT: Oscillatory-shear-flow-induced structures of a semidilute polymer solution of ultrahigh molecular weight deuterated polystyrene in dioctyl phthalate were investigated by using the small-angle light scattering (SALS) and the small-angle neutron scattering (SANS). Under a fixed strain amplitude of oscillatory shear flow at 4.8, we observed the shear-induced structures as a function of the angular frequency (ω) and the strain-phase. At low ω, butterfly patterns, which are the scattering patterns unique to the shear-induced structures formed in semidilute polymer solution, were observed by SALS and isotropic patterns with weak scattered intensities were obtained by SANS. At high ω, on the other hand, SANS showed butterfly patterns and SALS showed almost isotropic patterns. These results indicate that the anisotropic structures developed under oscillatory shear flow become smaller with increasing ω. From the SALS and SANS patterns, we obtained scattering profiles parallel and perpendicular to the flow direction. At ω higher than 0.6133 rad/s, the SANS profiles parallel to the flow direction could be reproduced by a linear combination of the squared Lorentzian (SQL) function, which reflects the scattering from the random two-phase structures, and the Ornstein−Zernike (OZ) function, which gives the scattering from concentration fluctuations in a single phase. This analysis suggests that the shear-induced structures are not just the concentration fluctuations in a single phase but kind of phase-separated structures having well-defined interfaces between two phases.

I. Introduction

A semidilute polymer solution undergoes a dramatic change when shear flow is imposed. A system that is homogeneous in a single phase without shear flow exhibits strong concentration fluctuations or phase separation at the shear rate, $\dot{\gamma}$, larger than the critical shear rate $\dot{\gamma}_c$.[1−3] This shear-induced enhancement of concentration fluctuations or phase separation has been extensively studied from the theoretical and experimental points of view, because this is regarded as a new research issue in statistical mechanics of open nonequilibrium systems.

Pioneering work in the theoretical field was done by Helfand and Frederickson,[4] who proposed that shear-induced enhancement of concentration fluctuations is caused by the coupling between concentration fluctuations and stress as a result of the concentration dependence of viscosity and normal stress coefficients. In addition, Onuki introduced a tensor variable to represent chain deformation and suggested a dynamic model to apply to this phenomenon.[5−7] After their works, several theoretical developments and modifications have been made in order to close the gap between the experimental results and the theories.[8−12]

Experimentally, there have been a large number of reports on this subject made by using small-angle light scattering (SALS),[1,13−21] small-angle neutron scattering (SANS),[22−25] shear−optical microscopy,[26] rheology measurement,[21,27−30] shear−dichroism, and shear−birefringence.[27,29,31,32,47] Among these experimental methods, the shear−scattering techniques provide us a structure factor, from which we can extract some statistical properties of the structures such as the characteristic wavelength of structures, the magnitude of concentration fluctuations, the fractal characteristics, and so forth. These data are indispensable for understanding the physics underlying this phenomenon.

So far most of the scattering experiments performed were SALS under shear flow, and the shear-induced structures having a length scale comparable to the wavelength of visible light were explored. Judging from several reports,[3,13,33] SALS has the q range covering from 3×10^{-4} to 3×10^{-2} nm^{-1}, which corresponds to the length scale in real space from 0.21 to 21 μm. Here, q is the amplitude of the scattering wave vector defined as $q = |\mathbf{q}| = (4\pi/\lambda) \sin(\theta/2)$, where λ is the wavelength of the incident beam and θ is the scattering angle in the medium used. In semidilute polymer solutions, one can picture this length scale as an assembly of the mesh structures or a "transient gel" comprised of many chains. We observed a highly anisotropic scattering pattern in the $q_x - q_z$ plane by using a cone−plate fixture made of quartz,[1−3] where the incident light was sent along the q_y direction. Here, x, y, and z axes are flow direction, velocity gradient direction, and vorticity or neutral direction, respectively, and q_x, q_y, and q_z denote the respective components of $\mathbf{q}$. This anisotropic scattering pattern is called a "butterfly pattern", which has also been observed for a uniaxially deformed gel by SANS.[34−36] Moreover, Wu et al.[13] gave their attention to the $q_x - q_y$ plane by using transparent coaxial cylinders. They

* To whom correspondence should be addressed.
[†] Kyoto University.
[‡] Present address: Sekisui Chemical Co., Ltd., 2-2, Kamichoshi-cho, Kamitoba, Minami-ku, Kyoto 601-8105, Japan.
[§] Japan Atomic Energy Research Institute.

10.1021/ma9910336 CCC: $19.00
Published on Web 02/23/2000

also found the butterfly pattern, but the shape of the butterfly and its pattern evolution with increasing shear rate was different from the results given by us.

In contrast to these SALS experiments, there have been only a few SANS experiments. SANS covers the q range from about 0.01 to 1 nm^{-1}, which corresponds to the length scale from 6.3 to 630 nm in real space. In this length scale, characteristics of a single chain and the size of the meshes made out of entangled polymer chains would be observed. Boué et al.[23] pointed out that the butterfly pattern appeared even in the SANS q region in the $q_x - q_z$ plane provided the shear rate is high enough. This butterfly pattern was observed in the low-q region of SANS, whereas they obtained an isotropic intensity distribution in the high-q region.

In those series of works, little attention had been given to the study using both SALS and SANS for given sets of experimental systems in order to unveil the structure factors over a extremely wide q range. In the present paper, we shall report some results obtained by a combination of SALS and SANS under a large amplitude oscillatory shear field for the first time. If we experimentally acquire a scattering intensity distribution or a structure factor of the shear-induced structures over a wide q range, not only the confirmation of the physical insight given by the theories that have been developed in the past decade but also exploration of the subjects that the theories cannot cover up to now would be possible. Moreover, in this work, we applied an oscillatory shear flow to induce structures, not a continuous shear flow as has been used in the most of the previous studies. As clarified in our previous paper,[40] the oscillatory shear flow has a strong merit: The oscillatory shear flow with frequency ω picks up only dominant Fourier modes of the concentration fluctuations having a relaxation rate comparable to ω, while the continuous shear flow with shear rate $\dot{\gamma}$ enhances those having relaxation rates smaller than $\dot{\gamma}$. This fact implies that the scattering peaks emerge in the structure factor under oscillatory shear flow. This information would play an important role in the further understanding of this phenomenon. To make the best use of the characteristics of the oscillatory shear flow, the newly developed flow−SALS apparatus[37] and the SANS data acquisition system[38] enable us to conduct, for the first time, dynamic measurements of the scattering structure factors as functions of strain amplitude, frequency, and the strain phase over a wide q range. This method is anticipated to experimentally clarify what kind of nonequilibrium structures are formed under oscillatory shear flow over a wide length scale, from microscopic scale to mesoscopic scale, or from a single-chain to many-chains dimension.

II. Experimental Methods

A. Sample. We employed a solution comprised of high molecular weight deuterated polystyrene (dPS) as a solute and dioctyl phthalate (DOP) as a solvent. The dPS used has a weight-average molecular weight (M_w) of 2.00×10^6, which was determined by the dynamic light scattering. The solution containing dPS of 8 wt % was prepared by dissolving dPS and DOP in excess methylene chloride and by evaporating methylene chloride completely. This is a semidilute solution with concentration c satisfying $c/c^* = 6.4$, c^* being the overlap concentration.[39] It is clearly recognized that the solution is in a single phase at 9 °C, at which all the experiments in this paper were carried out.

B. Phase-Resolved SALS Measurement. Light-scattering experiments were performed by a flow small-angle light-scattering (flow−SALS) apparatus, which enables us to carry out simultaneous measurements of SALS and rheological properties. The details of this apparatus used have been described elsewhere.[37] Here we shall describe only the essential part of this apparatus. Figure 1a shows a schematic diagram of the flow-SALS apparatus, where x, y, and z axis, respectively, correspond to the flow direction, the velocity gradient direction, and the vorticity (or neutral) direction. The shear cell consists of a cone and a plate made of quartz with radii of 40 mm and a cone angle of 1.0°. The cone-and-plate type shear cell containing the sample is covered by a temperature-controlled enclosure. A He−Ne laser with a wavelength of 632.8 nm was used as an incident beam source. The incident beam propagates along the velocity gradient direction. The scattered light is taken by a cooled charge coupled device (CCD) camera as a two-dimensional detector, the detecting plane of which is set parallel to the O_{xz} plane.

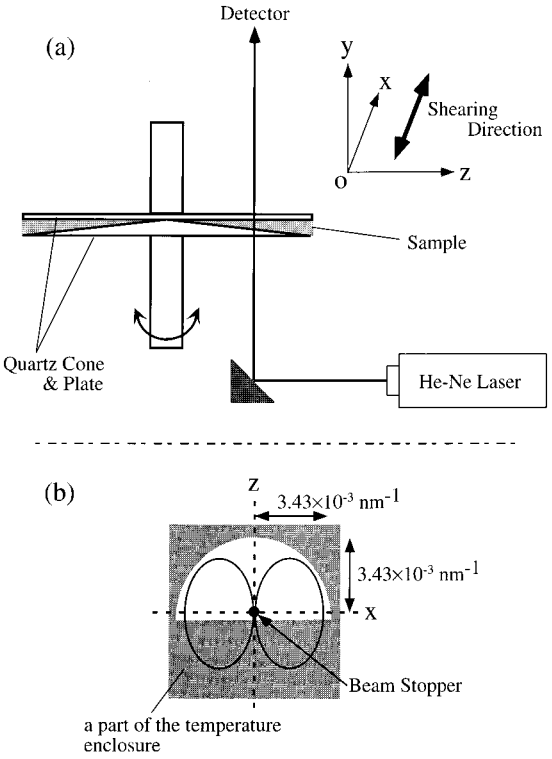

Figure 1. (a) Schematic diagram of the experimental set up. The Ox axis is parallel to the shearing direction, the Oy axis to the shear gradient direction, and the Oz axis to the vorticity or neutral direction. The incident beam was sent along the Oy axis, and the two-dimensional scattering pattern is detected by a CCD camera with its detector plane set parallel to the Oxz plane. (b) Due to the optical set up, q range for scattered light is limited inside the half circle with the radius of $q = 3.43 \times 10^{-3}$ nm^{-1}.

Because of the optical set up of this apparatus, the q range is limited. As shown in Figure 1b, the q range we can access exists inside the half circle with a radius of 3.43×10^{-3} nm^{-1}.

We applied the oscillatory shear flow given by the following equations as a function of frequency ω and time t.

$$\gamma(t) = \gamma_0 \sin \omega t = \gamma_0 \sin \phi \tag{1}$$

$$\dot{\gamma}(t) = \gamma_0 \omega \cos \omega t = \gamma_0 \omega \cos \phi \tag{2}$$

Here, γ, γ_0, $\dot{\gamma}$, and ϕ are, respectively, strain, strain amplitude, shear rate, and strain phase. When the oscillatory shear flow enhances the concentration fluctuations, the scattering intensity develops with t or ϕ. In about 20 min after applying the shear flow, the scattering intensity at a given ϕ became stationary and independent of the number of cycles. We refer to this state as a dynamic steady state hereafter. We measured the two-dimensional scattering pattern at a particular strain

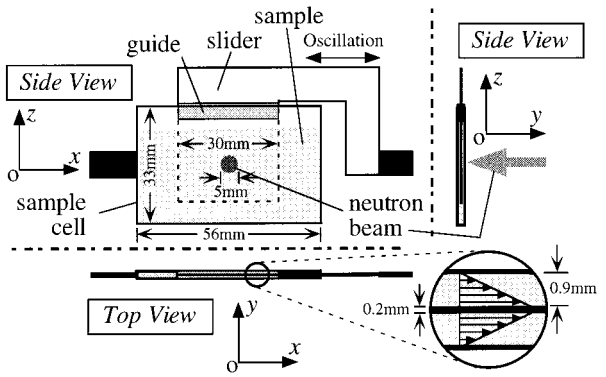

Figure 2. Schematic diagram of the shear cell used for SANS. The incident neutron beam was sent along the velocity gradient direction (along the *y* direction), and the 2D detector for SANS is set normal to the *y* axis.

phase interval between $\phi - \Delta\phi$ and $\phi + \Delta\phi$ at the dynamic steady state. $\Delta\phi$ was varied, depending on the relation between the exposure time of the CCD camera ($\Delta\phi = 0.3515°$ for $\omega = 0.06133$ rad/s, $\Delta\phi = 3.515°$ for $\omega = 0.6133$ rad/s, $\Delta\phi = 17.58°$ for $\omega = 6.133$ rad/s, and $\Delta\phi = 35.16°$ for $\omega = 12.27$ rad/s) and the period of the shearing cycle. The data acquisition was conducted under the condition where the incident laser intensity and the scattering volume keep the constant values during the experiment. The data were corrected so that the accumulated times of the CCD camera become the same with respect to each other. Hence the SALS intensity to be presented can be compared each other. The two-dimensional data were sector-averaged parallel and perpendicular to the flow direction with the azimuthal angle of ±5° in order to obtain scattering profiles as a function of q. We also obtained the sector-averaged profiles parallel and perpendicular to the flow direction for the data at the quiescent state. The scattering excess from the quiescent state was obtained by subtracting the scattering under shear flow from the scattering in the quiescent state.

C. Phase-Resolved SANS Measurement. The SANS experiments were carried out using a 20m SANS instrument (SANS-J) at the JRR-3M research reactor of the Japan Atomic Energy Research Institute (JAERI) in Tokai, Japan. The incident neutron beam has the wavelength of $\lambda = 10.44$ Å. With the sample-to-detector distance of $L = 2$m and 10m, the effective q range of $1.88 \times 10^{-2} \le q \le 7.62 \times 10^{-1}$ nm^{-1} was covered in this experiment.

Figure 2 shows a schematic diagram of the shear cell used for SANS. This sandwich-type shear cell imposes oscillatory shear flow on the solution by moving the slider, placed at the center of the cell, which is operated by a servo-controlled hydraulic deformation device. The cell is made of copper having a thickness of 0.2 mm. The incident neutron beam was sent along the velocity gradient direction, by which we could observe the same plane in the reciprocal space as the SALS experiment.

The phase-resolved data acquisition was performed by the *Dynamic Data Acquisition System* (*DDAS*),[38] which we recently developed. The two-dimensional scattering intensity, detected by a two-dimensional Riso-type detector, was integrated at a particular strain phase interval between $\phi_{i+1} - \phi_i = 360°/32 = 11.25°$, where ϕ_i is defined as $\phi_i \equiv 11.25i°$ ($i = 0,1, ..., 31$). Since the scattered neutron intensity was quite weak, all of the phase-resolved integrated data were accumulated over a large number of cycles so that the total time for each measurement of a given experimental condition becomes 5 h for $L = 2$ m, or 10 h for $L = 10$ m. The data at the quiescent state were circularly averaged to obtain the scattering intensity profiles as a function of q, and the SANS data under oscillatory shear flow were sector averaged, as for the SALS data under oscillatory shear flow, with the azimuthal angle of ±15°.

D. Rheology. Measurement of the linear viscoelasticity was carried out with ARES−FS (Rheometric Scientific Co. Ltd.) by using a cone-plate fixture with radii of 25 mm and a cone angle of 0.04 rad.

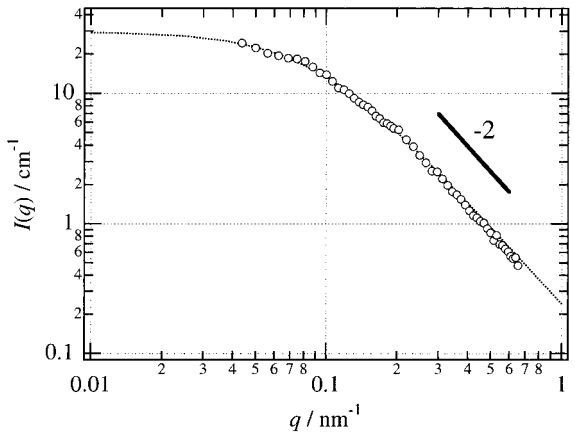

Figure 3. SANS profile from the semidilute solution at the quiescent state. The open circles denote the observed profile, and the dotted line is the best-fitted OZ function with ξ_f of 11.1 nm.

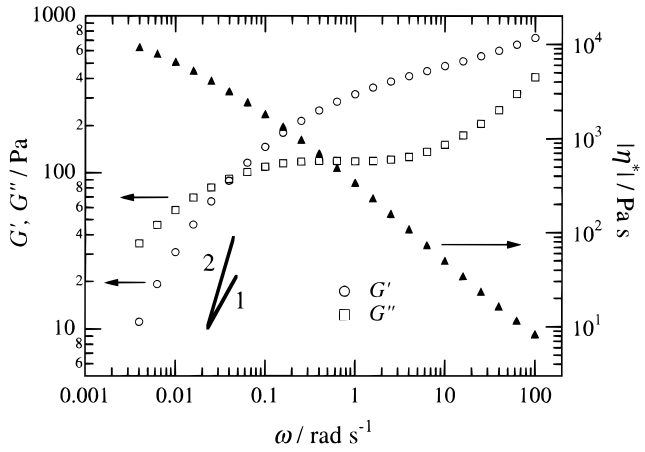

Figure 4. Linear viscoelastic properties of the semidilute solution as a function of angular frequency ω: G' (open circles), G'' (open squares) and $|\eta^*|$ (filled triangles).

III. Results

A. Static Properties. We first show the static properties of the semidilute solution examined by SANS. Figure 3 shows the SANS intensity profile as a function of q at the quiescent state (open circles). At the quiescent state, the system is in a single phase, and hence the scattering intensity can be described by the Ornstein−Zernike (OZ) function

$$I_{OZ}(q) = \frac{I_{OZ}(q=0)}{1 + \xi_f^2 q^2} \tag{3}$$

where ξ_f is a correlation length for the thermal concentration fluctuations. The dotted line indicates the OZ function best fitted with the experimental scattering profile. The measured intensity can be very well expressed by the OZ function, with the power law of q^{-2} in the q region higher than 0.2 nm^{-1}. ξ_f calculated by the fitting is 11.1 nm.

B. Linear Viscoelastic Properties. Figure 4 shows the linear viscoelastic properties as a function of ω. The applied strain amplitude is 0.2, which is within the limits of linear viscoelasticity. It should be pointed out that the terminal region, which is characterized by the

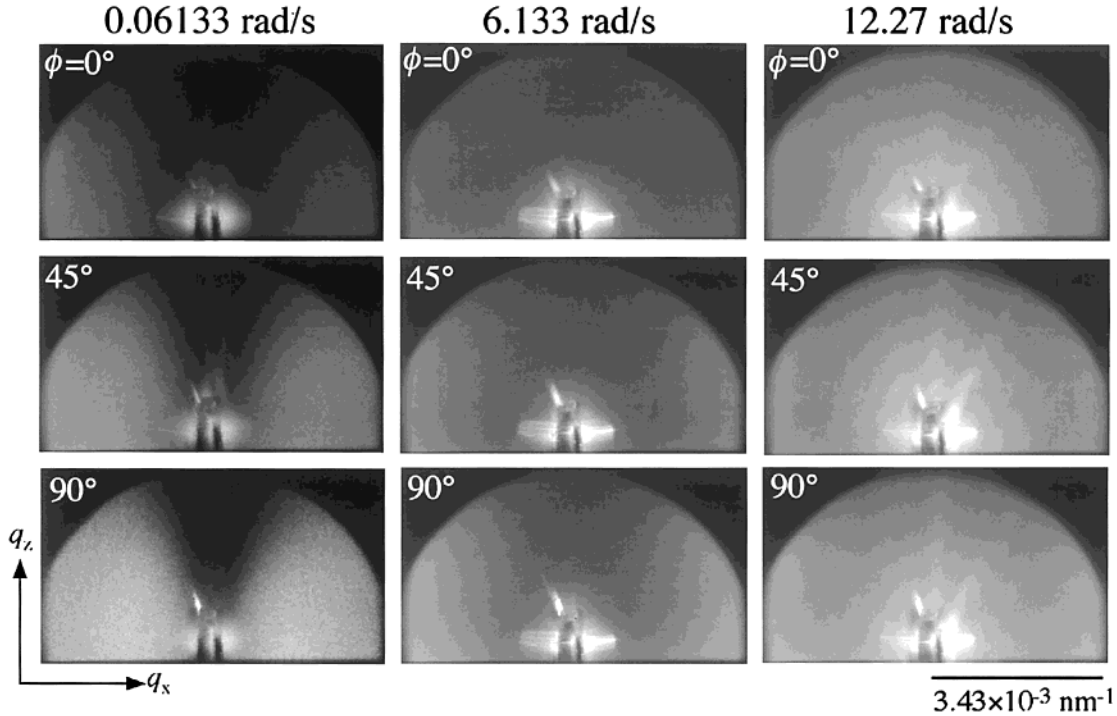

Figure 5. SALS patterns obtained at $\omega = 0.06133$, 6.133, and 12.27 rad/s and at representative ϕ (0, 45, and 90°) for a fixed value of $\gamma_0 = 4.8$.

power laws $G' \sim \omega^2$ and $G'' \sim \omega^1$, is not observed at the low ω region covered in this experiment. We expect the region may exist at $\omega < 0.001$ rad/s.

C. SALS Patterns. Figure 5 shows the light-scattering patterns taken under the oscillatory shear flow of $\omega = 0.06133$, 6.133, and 12.27 rad/s and at representative ϕ (0, 45, and 90°). The given γ_0 was 4.8, the same for all the cases. At $\omega = 0.06133$ rad/s, the intensity distributions exhibit highly anisotropic patterns with strong intensities along the flow direction (horizontal direction), which are often called "butterfly patterns". The appearance of the butterfly patterns indicates that structures having a strong correlation along the flow direction are formed under shear flow. The change in the scattering intensity distribution with ϕ is the same as the results reported by our previous paper,[40] in which it is confirmed that the intensity distributions of butterfly pattern in a shearing cycle change in harmony with ϕ independently of ω: as ϕ increases from 0 to 90°, the scattering intensity parallel to the flow direction increases and the butterfly wings expand, resulting in sharpening of the "dark streak" perpendicular to flow, and as ϕ increases from 90 to 180°, on the other hand, the scattering intensity decreases and the dark streak broadens. These observations indicate that the shear-induced structures in a shearing cycle change in harmony with ϕ independently of ω: the shear-induced structures tend to develop from $\phi = 0$ to 90° and decay from 90 to 180°. While the change in scattering patterns from $\phi = 90$ to 180° are not shown here, the same tendency as that previously reported[40] was observed in this experiment.

At $\omega = 6.133$ rad/s, the shape of the butterfly is different from that at $\omega = 0.06133$ rad/s. The scattering pattern at $\phi = 0°$ is almost isotropic and the scattering intensity perpendicular to the flow direction is higher than that at $\omega = 0.06133$ rad/s. Moreover, the increase in the scattering intensity in the high q_x region from $\phi = 0$ to 90° is not as remarkable as that at $\omega = 0.06133$ rad/s, and the scattering intensity in the low q region does not change with ϕ. The butterfly at $\omega = 6.133$ rad/s and at $\phi = 90°$ has a scattering maximum along q_x at the large q_x limit of our q window of observation, much larger than the q_x value where the butterfly at $\omega = 0.06133$ rad/s and at $\phi = 90°$ has the maximum intensity.

At $\omega = 12.27$ rad/s, we cannot recognize the anisotropy of the scattering patterns, although in fact the intensity in the high q_x region is slightly higher than that in the high q_z region as will be shown in the scattering profile later. The q_x value where the butterfly has a maximum intensity may exist outside our q window.

D. SANS Patterns. Figure 6 shows the SANS patterns obtained under the same oscillatory shear flow conditions as those in the SALS experiments. The patterns at the representative ϕ between 0° and 180° are presented. The patterns at $\omega = 0.06133$ rad/s, at which the clear butterfly patterns were observed with SALS experiment (Figure 5), were almost isotropic, and the changes in the pattern and intensity with increasing ϕ could not be discerned. At 6.133 rad/s, the changes in the scattering intensity and pattern with ϕ were not also observed clearly. However, compared with the patterns at $\omega = 0.06133$ rad/s, the intensity level increased, and the patterns in the low-q region were elliptical with a major axis parallel to the flow direction (horizontal direction in Figure 6), indicating the anisotropic structures were formed even in the SANS q-scale. At $\omega = 12.27$ rad/s, the intensity level increased further, and butterfly patterns appeared in the low-q region. The butterfly clearly emerged at $\phi = 0°$. As ϕ increases from 0 to 90°, the butterfly pattern was shrinking along the flow direction. As ϕ increased from 90 to 180°, on the other hand, the butterfly wings expanded. This behavior qualitatively indicates that the shear-induced structures developed with ϕ increasing from 0 to 90°, and decayed from 90 to 180°.

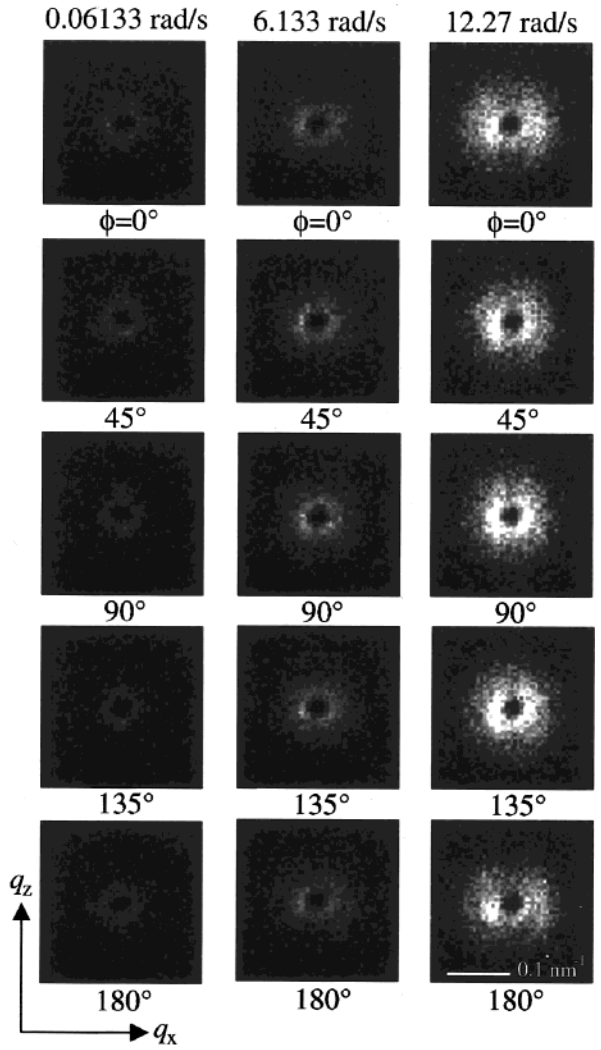

Figure 6. SANS patterns obtained at $\omega = 0.06133$, 6.133, and 12.27 rad/s and at representative ϕ (0, 45, 90, 135, and 180°) for a fixed value of $\gamma_0 = 4.8$.

E. SALS and SANS Profiles Parallel and Perpendicular to the Flow Direction. To evaluate the scattering intensity more quantitatively, we shall focus on the scattering profiles parallel and perpendicular to the flow direction obtained by SALS and SANS. Figure 7 shows the scattering profiles parallel to the flow direction as a function of q_x at representative ϕ (0 and 90°). The SALS profiles were equally multiplied by a shift factor in order to compare them with SANS profiles, although the SANS profiles retain the corrected values with the absolute units (cm^{-1}). The dotted lines between the two sets of the profiles are the visual guides for clarifying the correspondence between SALS and SANS profiles at the same ω. Since the ω dependence of SALS profiles are somewhat complicated, we shall concentrate on the scattering peaks. Although some of the peaks exist out of our q range covered by both SALS and SANS, we can deduce the existence of the scattering peaks from the shape of the scattering profiles, and trace the peak positions as well. For both ϕ, the scattering peaks in the SALS q region appeared to move to a higher q region as ω increased. This tendency, especially clear at $\phi = 90°$, is a good indication that the characteristic wavelength of shear-induced structures becomes smaller with increasing ω, which we have already reported in the previous paper.[40]

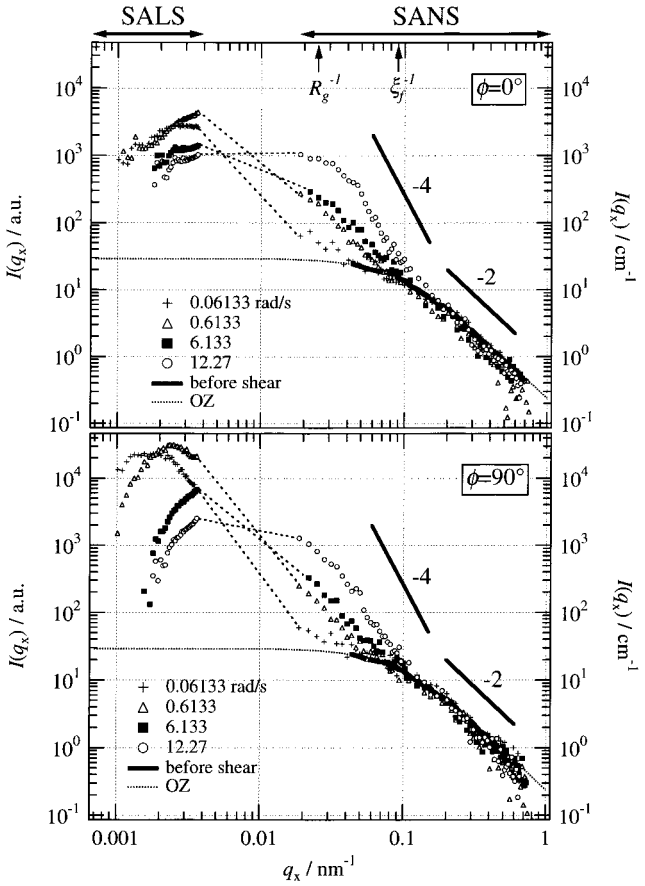

Figure 7. Scattering profiles parallel to the flow direction at $\phi = 0$ (upper) and 90° (lower) obtained by SALS (left axis) and SANS (right axis). The SALS profiles were equally multiplied by a shift factor in order to compare them with SANS profiles, although the SANS profiles remain the corrected values with the absolute units (cm^{-1}). The doted lines are visual guides for clarifying the connection between SALS and SANS intensities. $\gamma_0 = 4.8$.

The ω dependence of scattering profiles in the SANS q region is simple. In the q region higher than about 0.1 nm^{-1}, the intensity level at all ω remained in the level at the quiescent state with the power law of $I(q_x) \sim q_x^{-2}$ for both ϕ. In the q region lower than about 0.1 nm^{-1}, the intensity level became higher with increasing ω. It should be noticed that the profiles at $\omega = 12.27$ rad/s for both ϕ showed the power law with an exponent of nearly -4 ($I(q_x) \sim q^{-4}$).

Figure 8 shows the scattering profiles perpendicular to the flow direction as a function of q_z. Again, the dotted lines drawn between SALS and SANS profiles are visual guides. The SALS data at $\omega = 0.06133$ rad/s was omitted, because there was no excess scattering from the quiescent state. However, the data are expected to follow the OZ function (i.e., on the dotted line shown in Figure 8). Except for the profiles at $\omega = 0.06133$ rad/s, the intensity excess from the quiescent state was observed in the q_z region to be smaller than about 0.1 nm^{-1}. The intensity level in this q_z region simply increased with an increase of ω. In the q_z region higher than about 0.1 nm^{-1}, the intensity was almost the same as that at the quiescent state, the tendency of which is the same that as the profiles parallel to the flow direction.

To compare $I(q_x)$ and $I(q_z)$ at the same ω, the scattering profiles shown in Figures 7 and 8 were rear-

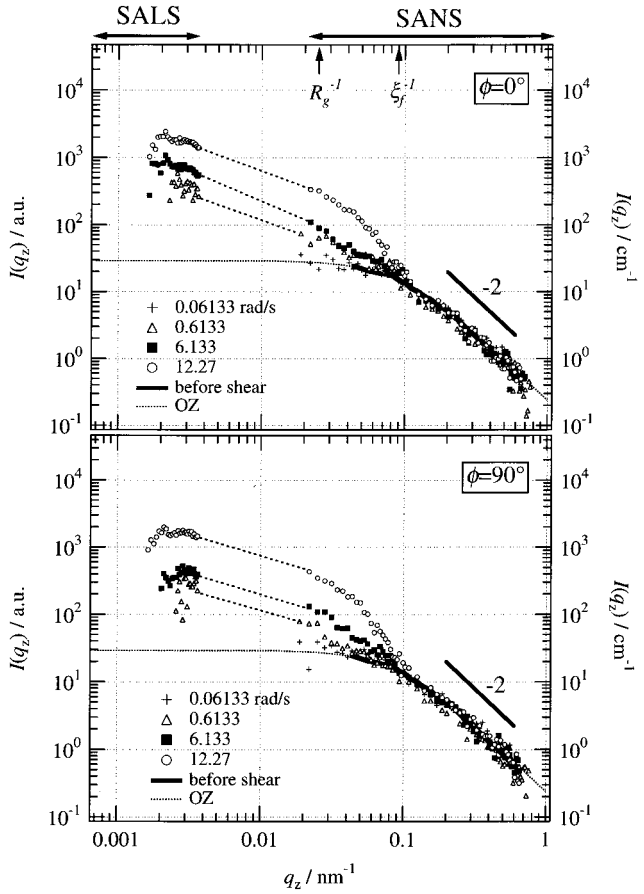

Figure 8. Scattering profiles perpendicular to the flow direction at $\phi = 0$ (upper) and 90° (lower) obtained by SALS (left axis) and SANS (right axis). $\gamma_0 = 4.8$.

ranged in Figure 9. Here we focus on the profiles only at $\phi = 90°$. For all ω, in the q region smaller than about 0.06 nm^{-1}, the scattering intensity parallel to the flow direction exceeds those perpendicular to the flow direction,[41] indicating anisotropic structures having the strong correlation along the flow direction are formed in this q scale. On the other hand, in the q region larger than about 0.06 nm^{-1}, the intensity level parallel and perpendicular to the flow direction is the same. In particular, at $\omega = 6.133$ and 12.27 rad/s, in the q region between about 0.06 and 0.1 nm^{-1}, the two sets of the scattering intensities are the same, but the intensity level is larger than the OZ level. This implies that the isotropic structures are induced even under the oscillatory shear flow in this q-scale, although this q region is quite narrow. In the q region larger than 0.1 nm^{-1}, the scattering intensities are the same as the OZ level, indicating the shear flow did not affect the structures reflected in this q region.

IV. Discussions

A. ω Dependence of Shear-Induced Structures. The scattering profiles given in Figures 7 and 8 bear two crucial features: (a) as ω increased, the scattering peak along the flow direction q_{mx} moved to a higher q_x region; (b) as ω increased, the scattering intensity in the SANS q region smaller than about 0.1 nm^{-1} also increased for both directions, while the intensity in the q region higher than about 0.1 nm^{-1} remained at that level in the quiescent state. Here, we would interpret these two features in terms of the "solvent squeezing",[5−7,40] which could give a qualitative explanation for the

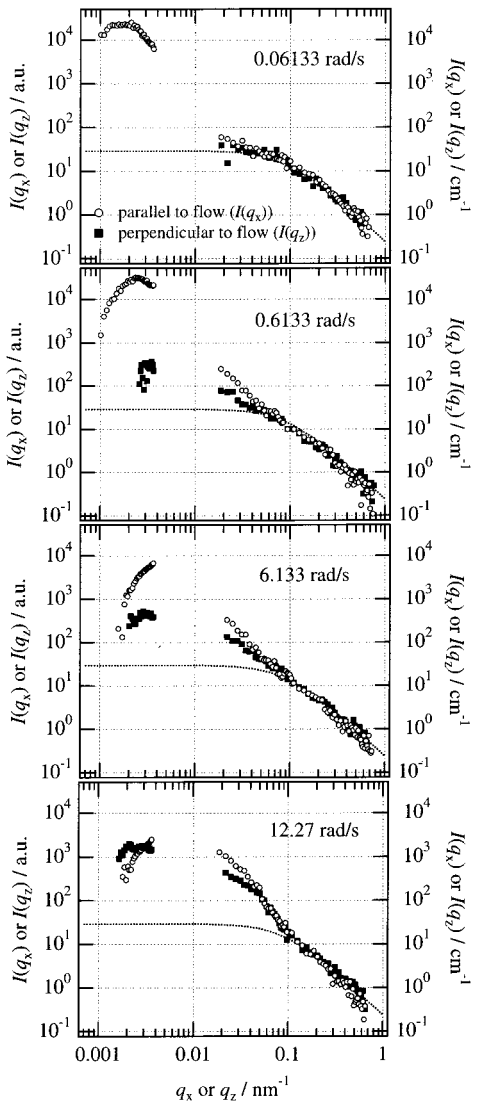

Figure 9. Comparison of the scattering profiles parallel and perpendicular to the flow direction at the same ω. The scattering profiles shown in Figures 7 and 8 were rearranged.

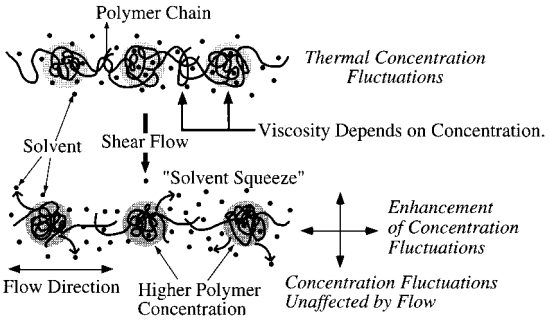

Figure 10. Schematic representation of the origin of the shear-induced structure formation.

mechanism of the formation of the shear-induced structures in semidilute polymer solution. Therefore, we shall briefly review the picture of the solvent squeezing.

The models explaining the formation of shear-induced structures are schematically depicted in Figure 10. In a semidilute polymer solution in the quiescent state, there are thermal concentration fluctuations, giving rise to the regions which have higher polymer concentrations and hence have more entanglement points and those

which have lower polymer concentrations and hence less entanglement points. When shear flow is imposed on such a system, the stress level tends to become higher in more entangled regions compared with less entangled regions, due to the concentration dependence of the viscosity. This effect is often referred to as the coupling between concentration fluctuations and stress. The stress level or the free energy stored by elastic deformation of the entangled polymer chains is relaxed by disentanglement when the shear rate $\dot{\gamma}$ is lower than the terminal relaxation rate τ_m^{-1}. However, if $\dot{\gamma}$ is higher than τ_m^{-1}, the elastic free energy is released only by the "solvent squeezing" from the more entangled regions. The higher the concentration, the larger the stored elastic free energy and hence the more is the solvent squeezing. As a result, the concentration fluctuations or phase separation are built up under shear flow, provided $\dot{\gamma}$ is larger than the critical shear rate $\dot{\gamma}_c$ of the system ($\dot{\gamma}_c \sim \tau_m^{-1}$). If $\dot{\gamma}$ is increased further above $\dot{\gamma}_c$, the shear-induced phase separation is eventually brought about.

This model can be applied to the system under both the continuous shear flow and the oscillatory shear flow. In the case of the continuous shear flow, all the Fourier modes of the concentration fluctuations having $\tau^{-1}(\Lambda) < \dot{\gamma}$ are affected, or rather enhanced, because they are deformed before they decay. Here Λ is the wavelength of the Fourier mode of the concentration fluctuations and $\tau^{-1}(\Lambda)$ is the relaxation rate of the concentration fluctuation having Λ. In other words, Fourier modes with Λ greater than Λ_c are affected by shear, where Λ_c satisfies $\tau^{-1}(\Lambda_c) = \dot{\gamma}$. The higher the value of $\dot{\gamma}$, the smaller the value of Λ_c and hence the wider the range of the Fourier modes which are affected by shear. This effect qualitatively explains the experimental results that the butterfly pattern developed with increasing $\dot{\gamma}$ in such a way that the intensity level increased, the butterfly wings opened, and the dark streak narrowed, which have been already found.[2,3]

On the other hand, when an oscillatory shear flow with a frequency ω is imposed on the system, only the Fourier modes of concentration fluctuations having $\tau^{-1}(\Lambda) \sim \omega$ would be dominantly affected. This is because the Fourier modes of the concentration fluctuations having $\tau^{-1}(\Lambda) \gg \omega$ decay via disentanglement before they are deformed by the shear flow, and hence they are unaffected by shear, while the Fourier modes of the concentration fluctuations having $\tau^{-1}(\Lambda) \ll \omega$ cannot respond to the applied shear flow in a sense that the concentration fluctuations cannot be enhanced as a result of the solvent squeezing. This is simply because under this situation the entangled networks are just deformed and relaxed reversibly without the solvent squeezing. This characteristic of oscillatory shear flow brings about the scattering peaks in the flow direction shown in Figure 7.

On the basis of the above discussion, we try to qualitatively interpret the ω dependence of the structures. We can think of the characteristic length of structures Λ_{mx} developed under the oscillatory shear, which is given by $\Lambda_{mx} = 2\pi/q_{mx}$. Although the observed q_{mx} changed with ϕ, we shall give our attention to the q_{mx} at a given ϕ. Since the Fourier mode of the concentration fluctuations affected by the oscillatory shear flow with angular frequency of ω would have a wavelength on the order of Λ_{mx}, we have $\tau^{-1}(\Lambda) = \tau^{-1}(\Lambda_{mx}) \sim \omega$. Although the flow of the solvent in the process of the solvent squeezing is a complex phenomenon, we assume that this process is not so different from the cooperative diffusion mode at the equilibrium state,[42] giving rise to the relation $\Lambda_{mx} \cong (D_{coop}t)^{1/2}$, where D_{coop} is the cooperative diffusion constant and t is the time available for the diffusion of the length of Λ_{mx}.

Now we can consider two directions of the solvent flow at the dynamic steady state: One is the flow against the osmotic pressure gradient, which develops the structures. Another is the flow along the osmotic pressure gradient, which makes the structures decay. As described earlier, the shear-induced structures in a shearing cycle develop and decay in harmony with ϕ, hence the time given for the former process in a shearing cycle is a quarter of a cycle, that is, $\pi/2\omega$. We are now concerned with the structural development in the former process; then, we have $\Lambda_{mx} \approx (\pi D_{coop}/2\omega)^{1/2}$. This qualitative relation gives an interpretation of the ω dependence of the structures. As ω increases, Λ_{mx} decreases, and then q_{mx} moves to the higher q_x region. This is consistent with the observed shift of q_{mx}, and is also consistent with the increase of the scattering intensity in the SANS q region because the whole distribution of the structures around Λ_{mx} also moves to the high-q region.

We estimate Λ_{mx} by using the relation introduced above. The semidilute PS/DOP system has $D_{coop} \sim 10^5$ nm^2 s^{-1},[43] hence we can obtain the following values of Λ_{mx} and q_{mx}: for $\omega = 0.06133$ rad/s, $\Lambda_{mx} \approx 1.6$ μm, and $q_{mx} \approx 3.9 \times 10^{-3}$ nm^{-1}; for $\omega = 12.27$ rad/s, $\Lambda_{mx} \approx 0.11$ μm, and $q_{mx} \approx 5.6 \times 10^{-2}$ nm^{-1}. These values are close to the observed values of q_{mx}, indicating the validity of the above arguments.

Let us now focus on the scattering intensity in the q region higher than about 0.1 nm^{-1}. There is a critical $q = q_c \approx 0.1$ nm^{-1}, above which the intensity distribution is almost independent of ϕ and ω and has no anisotropy. It is worth noting that q_c is almost independent of ω, and almost identical with ξ_f^{-1} in the quiescent state as indicated in Figures 7 and 8. In other words, one can safely state that the static properties of the structures having a characteristic length scale larger than ξ_f are affected by shear flow, but those smaller than ξ_f are not affected by shear flow, because we could regard ξ_f as the distance between entangled points (mesh size) formed by two or more different chains. This indicates that the shear-induced structures formed via the solvent squeeze involve a long-range topological rearrangement of the entangled networks due to the solvent squeezing without changing the local structure of the networks having length scale smaller than the mesh size.

B. A Possible Analysis of SANS Profiles. At this stage, we present a possible analysis of the excess scattering observed in SANS. We postulate that the structures induced by the oscillatory shear flow are a kind of distinct phase-separated structures, with clear interfaces between two phases. This postulate strongly implies that the observed scattering profile can be expressed by a linear combination of two scattering functions, i.e., an OZ function, which has appeared in eq 1, and a squared Lorentzian (SQL) function given by the following equation.[44−46]

$$I_{SQL}(q) = \frac{I_{SQL}(q=0)}{(1 + \xi_d^{\,2} q^2)^2} \tag{4}$$

An OZ function reflects the scattering from the concen-

tration fluctuations inside the phase-separated domains, and a SQL function expresses the scattering of the random two-phase structures with a sharp interface.[44−46] Here the random two-phase structures refer to the structures with the random distribution in location and size of each domain. We will try to reproduce the observed SANS profiles presented in Figure 7 by using the linear combination of eqs 3 and 4.

Since eqs 3 and 4 can be applied only for the isotropic system, we have to generalize these equations for the anisotropic system. The scattering theory for the oriented random two-phase system has been already derived by one of us,[46] giving the following equation:

$$I_{\mathrm{SQL}}(\mathbf{q}) = K\langle\eta^2\rangle(\xi_{\parallel})_{\mathrm{d}}(\xi_{\perp})_{\mathrm{d}}{}^2F(x) \tag{5}$$

with

$$F(x) = \frac{1}{(1+x^2)^2} \tag{6}$$

and

$$x = \sqrt{q_x{}^2(\xi_{\parallel})_{\mathrm{d}}{}^2 + q_y{}^2(\xi_{\perp})_{\mathrm{d}}{}^2 + q_z{}^2(\xi_{\perp})_{\mathrm{d}}{}^2} \tag{7}$$

where K is a proportionality constant, $\langle\eta^2\rangle$ is the mean-squared fluctuations of scattering contrast, and $(\xi_{\parallel})_{\mathrm{d}}$ and $(\xi_{\perp})_{\mathrm{d}}$ are, respectively, the correlation lengths of the oriented random two-phase structures parallel and perpendicular to the flow direction. In this calculation, we assumed that the shape of the correlation function has an axial symmetry, where the major axis is parallel to the flow direction with the correlation length of $(\xi_{\parallel})_{\mathrm{d}}$ and the correlation lengths along the y and z direction equal to $(\xi_{\perp})_{\mathrm{d}}$. Here we are concerned with the scattering profiles along the x or z direction. As for the scattering profile along the x direction, we can put $q_y = q_z = 0$, giving

$$I_{\mathrm{SQL}}(q_x) = \frac{K\langle\eta^2\rangle(\xi_{\parallel})_{\mathrm{d}}(\xi_{\perp})_{\mathrm{d}}{}^2}{[1 + q_x{}^2(\xi_{\parallel})_{\mathrm{d}}{}^2]^2} \tag{8}$$

$$= \frac{I_{\mathrm{SQL}}(q_x = 0)}{[1 + q_x{}^2(\xi_{\parallel})_{\mathrm{d}}{}^2]^2} \tag{9}$$

and as for the scattering profile along the z direction, $q_x = q_y = 0$, giving

$$I_{\mathrm{SQL}}(q_z) = \frac{K\langle\eta^2\rangle(\xi_{\parallel})_{\mathrm{d}}(\xi_{\perp})_{\mathrm{d}}{}^2}{[1 + q_z{}^2(\xi_{\perp})_{\mathrm{d}}{}^2]^2} \tag{10}$$

$$= \frac{I_{\mathrm{SQL}}(q_z = 0)}{[1 + q_z{}^2(\xi_{\perp})_{\mathrm{d}}{}^2]^2} \tag{11}$$

On the other hand, as shown in Figures 7−9, the scattering profiles observed in the q region larger than 0.1 nm^{-1} keep the OZ form without anisotropy, indicating $(\xi_{\parallel})_{\mathrm{f}} = (\xi_{\perp})_{\mathrm{f}} \equiv \xi_{\mathrm{f}}$ where $(\xi_{\parallel})_{\mathrm{f}}$ and $(\xi_{\perp})_{\mathrm{f}}$ are, respectively, the correlation length parallel and perpendicular to the flow direction for the thermal concentration fluctuations inside the phase-separated domains. Hence we can still use eq 3 for this calculation. From eqs 3, 9, and 11 we finally have the following scattering functions:

$$I(q_x) = \frac{I_{\mathrm{SQL}}(q_x = 0)}{[1 + q_x{}^2(\xi_{\parallel})_{\mathrm{d}}{}^2]^2} + \frac{I_{\mathrm{OZ}}(q_x = 0)}{1 + q_x{}^2\xi_f{}^2} \tag{12}$$

$$I(q_z) = \frac{I_{\mathrm{SQL}}(q_z = 0)}{[1 + q_z{}^2(\xi_{\perp})_{\mathrm{d}}{}^2]^2} + \frac{I_{\mathrm{OZ}}(q_z = 0)}{1 + q_z{}^2\xi_f{}^2} \tag{13}$$

The observed SANS profiles and the results of data fitting along the x-direction are shown in Figure 11. The profiles at 0.6133 and 6.133 rad/s are arbitrarily shifted along the vertical direction. The practical procedure regarding the decomposition of the observed profile into the SQL and OZ function is as follows. In the high q_x region, the contribution from the concentration fluctuation inside the domain to the net scattering dominates the contribution from the phase-separated domain, and hence the observed profile in high q_x region was best fitted with the OZ function, which are shown with the dotted curve. The residual intensity, i.e., the intensity difference between the observed and the best-fitted OZ intensities, was best fitted with the SQL function, which was denoted with the dashed−dotted curve. The solid curve shows the linear combination of the calculated SQL and OZ functions. This procedure was conducted for each profile.

At 0.6133 and 6.133 rad/s, the fitting is almost perfect for both $\phi = 0$ and 90°. At 12.27 rad/s, the agreement between the observed intensity and the calculated function is also fine, though the observed profiles show downward deviation in the low-q_x region. We have already observed in Figure 7 that the scattering peak at 12.27 rad/s originated from the interdomain interference exists just outside of the small q-limit of our SANS optics. This causes the observed downward deviation from the SQL function.

The intensity difference between the observed and the calculated OZ intensities, which is defined as $I_{\mathrm{d}}(q_x)$, is shown in Figure 12. $I_{\mathrm{d}}(q_x)$ purely reflects the contribution from the domain structures. These profiles show the $q_x{}^{-4}$ dependence (Porod law) except for the low-q_x side, due to the interdomain interference effects, indicating the existence of the sharp interfaces between two phases.

From the fitting with SQL function, we obtained $(\xi_{\parallel})_{\mathrm{f}}$. Meanwhile the scattering profiles show or suggest a periodicity of the structures $\Lambda_{mx} = 2\pi/q_{mx}$. To clarify the relation between these two lengths, the comparison between these two lengths has to be done. Only for the data obtained at $\omega = 0.6133$ rad/s and at $\phi = 90°$ (see Figure 7) can we compare Λ_{mx} with $(\xi_{\parallel})_{\mathrm{d}}$. From the fitting, $(\xi_{\parallel})_{\mathrm{d}}$ is 82.3 nm, and from the peak position of the scattering profile, Λ_{mx} is 2240 nm. Hence Λ_{mx} is about 27.3 times larger than $(\xi_{\parallel})_{\mathrm{d}}$. One of the possible situations explaining this analysis is that the shear-induced structures are the periodic superstructures with the periodicity of Λ_{mx} values, which are comprised of nonrandomly distributed primary structures having the size of $(\xi_{\parallel})_{\mathrm{d}}$.

On the other hand, the data fitting for the SANS profiles perpendicular to the flow direction by using eq 13 was not good, that is, the intensity difference between the observed intensity and the calculated OZ function did not show the q region that obeys the Porod law. Now we can only say that the contribution from the domain structure is very weak and is buried under the contribution of the concentration fluctuations inside each domain.

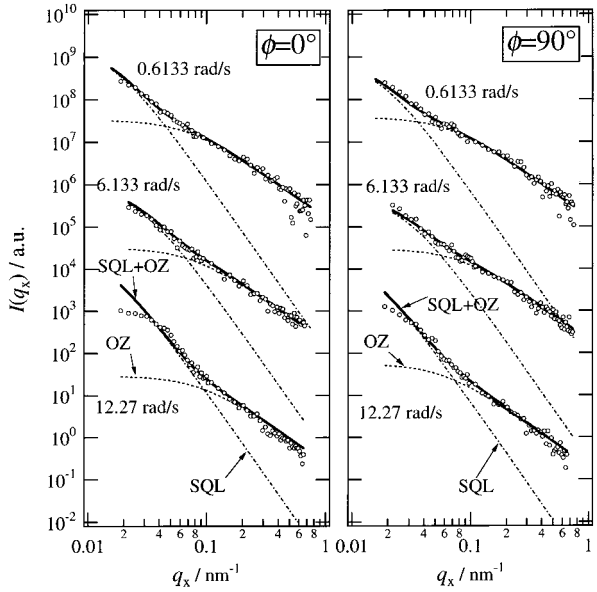

Figure 11. Reproduction of the SANS profiles parallel to the flow direction using a combination of an OZ function and a SQL function. The profiles at 0.6133 rad/s and 6.133 rad/s were arbitrary shifted along the vertical direction. The open circles are the observed intensity. The dotted lines, the dashed−dotted lines, and the solid lines are, respectively, the fitted OZ function, the fitted SQL function, and the combination of these two functions.

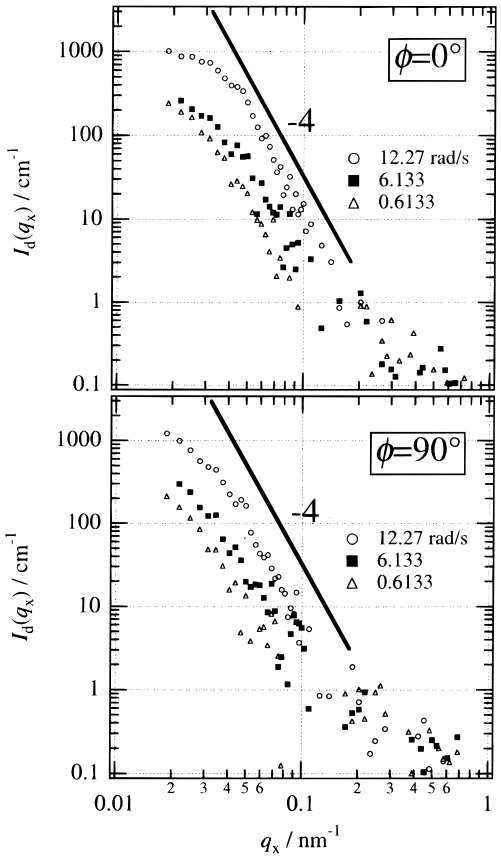

Figure 12. Residual intensity $I_d(q_x)$: the intensity difference between the observed SANS intensity and the fitted OZ function.

Here we have to notice that the butterfly patterns are never reproduced just by the combination of SQL and OZ functions, which predicts that the scattering intensities parallel and perpendicular to the flow direction approach the same value in the limit of $q = 0$ (eqs 8 and 10). In our analysis, the scattering intensity shows the feature of the SQL function only in the q region where the fitting is properly conducted. In the q region smaller than the q region where the fitting curve is observed to deviate from SQL, we consider that a scattering function other than SQL, giving the feature of the butterfly, is superimposed. If we can obtain this structure factor, we might reproduce the scattering intensity over the whole q region by the combination of OZ, SQL, and an unknown structure factor giving the butterfly characteristics. Experimentally we do not yet know whether the scattering intensities parallel and perpendicular to the flow direction approach the same value in the limit of $q = 0$.

From the analysis discussed above, it seems reasonable to suppose that the structures developed by the oscillatory shear flow are not just the concentration fluctuations in a single phase but instead reflect the distinct phase-separated structures having sharp interfaces between two phases. So far, it has been ambiguous whether the shear-induced structures in semidilute polymer solution reflect true "phase separation", because this term, as pointed out by Migler et al.,[30] has been defined only for quiescent systems. The system we have focused on in this paper is a nonequilibrium system since the shear flow as an external field continuously supplies the energy to the system. We do not know any definite criteria for the phase separation in the nonequilibrium state, but if we regard the existence of the interfaces as one of the evidences of the phase separation occurring in the system, this phenomenon is a shear-induced phase transition from the single-phase state to the two-phase state.

V. Conclusion

We have performed the light scattering and the small-angle neutron scattering to investigate the structures developed under the oscillatory shear flow in a semidilute polymer solution of high molecular weight deuterated polystyrene in dioctyl phthalate. The information on shear-induced structures at a particular strain phase over the wide q range could be obtained using the newly developed SALS apparatus and the DDAS at the SANS facility.

We observed the butterfly patterns in the SALS q region under the low-frequency oscillatory shear flow and in the SANS q region under the high-frequency oscillatory shear flow. Moreover, in the scattering profiles along the flow direction, the scattering peak due to the interdomain interference appeared. As the frequency increased, the scattering peak moved to the higher q region. These results could be explained by the following interpretation: the higher the frequency, the shorter the time available for the structure formation in a shearing cycle, and hence the smaller the structures become.

We also showed one of the possible interpretations of the SANS profiles. The SANS profiles could be reproduced by a linear combination of a SQL function and a OZ function, indicating that the shear-induced structure formation is a phase transition from the single-phase state to the two-phase state with a sharp interface.

References and Notes

(1) Hashimoto, T.; Takebe, T.; Fujioka, K. In *4th Nishinomiya-Yukawa Symposium on Theoretical Physics; Dynamics and*

Patterns in Complex Fluids; Onuki, A., Kawasaki, K., Eds.; Springer: Heidelberg, Germany, 1990; p 86.
(2) Hashimoto, T.; Fujioka, K. *J. Phys. Soc. Jpn.* **1991**, *60*, 356.
(3) Hashimoto, T.; Kume, T. *J. Phys. Soc. Jpn.* **1992**, *61*, 1839.
(4) Helfand, E.; Fredrickson, G. H. *Phys. Rev. Lett.* **1989**, *62*, 2468.
(5) Onuki, A. *Phys. Rev. Lett.* **1989**, *62*, 2472.
(6) Onuki, A. *J. Phys. Soc. Jpn.* **1990**, *59*, 3427.
(7) Doi, M.; Onuki, A. *J. Phys. II Fr.* **1992**, *2*, 1631.
(8) Milner, S. T. *Phys. Rev. E* **1993**, *48*, 3674.
(9) Ji, H.; Helfand, E. *Macromolecules* **1995**, *28*, 3869.
(10) Onuki, A. *J. Phys.: Condens. Matter* **1997**, *9*, 6119.
(11) Onuki, A.; Yamamoto, R.; Taniguchi, T. *J. Phys. II Fr.* **1997**, *7*, 295.
(12) Sun, T.; Balazs, A. C.; Jasnow, D. *Phys. Rev. E* **1997**, *55*, 6344.
(13) Wu, X.-L.; Pine, D. J.; Dixon, P. K. *Phys. Rev. Lett.* **1991**, *66*, 2408.
(14) Dixon, P. K.; Pine, D. J.; Wu, X.-L. *Phys. Rev. Lett.* **1992**, *68*, 2239.
(15) van Egmond, J. W.; Werner, D. E.; Fuller, G. G. *J. Chem. Phys.* **1992**, *96*, 7742.
(16) Wirtz, D. *Phys. Rev. E* **1994**, *50*, 1755.
(17) Wirtz, D. *Macromolecules* **1994**, *27*, 5639.
(18) Kume, T.; Asakawa, K.; Moses, E.; Matsuzaka, K.; Hashimoto, T. *Acta Polym.* **1995**, *46*, 79.
(19) Kume, T.; Hashimoto, T. In *Flow-Induced Structure in Polymers*; Nakatani, A. I., Dadmun, M. D., Eds.; American Chemical Society: Washington, DC, 1995; p 35.
(20) Murase, H.; Kume, T.; Hashimoto, T.; Ohta, Y.; Mizukami, T. *Macromolecules* **1995**, *28*, 7724.
(21) Kume, T.; Hattori, T.; Hashimoto, T. *Macromolecules* **1997**, *30*, 427.
(22) Hammouda, B.; Nakatani, A. I.; Waldow, D. A.; Han, C. C. *Macromolecules* **1992**, *25*, 2903.
(23) Boué, F.; Lindner, P. *Europhys. Lett.* **1994**, *25*, 421.
(24) Nakatani, A. I.; Douglas, J. F.; Ban, T.-B.; Han, C. C. *J. Chem. Phys.* **1994**, *100*, 3224.
(25) *ACS Symposium Series 597*, *Flow-Induced Structure in Polymers*; Nakatani, A. I., Dadmun, M. D., Eds.; American Chemical Society: Washington, DC, 1995.
(26) Moses, E.; Kume, T.; Hashimoto, T. *Phys. Rev. Lett.* **1994**, *72*, 2037.
(27) Yanase, H.; Moldenaers, P.; Mewis, J.; Abetz, V.; van Egmond, J.; Fuller, G. G. *Rheol. Acta* **1991**, *30*.
(28) Magda, J. J.; Lee, C. S.; Muller, S. J.; Larson, R. G. *Macromolecules* **1993**, *26*, 1696.
(29) Fuller, G.; van Egmond, J.; Wirtz, D.; Peuvrel-Disdier, E.; Wheeler, E.; Takahashi, T. In *Flow-Induced Structure in Polymers*; Nakatani, A. I., Dadmun, M. D., Eds.; American Chemical Society: Washington, DC, 1995; p 22.
(30) Migler, K.; Liu, C.; Pine, D. J. *Macromolecules* **1996**, *29*, 1422.
(31) van Egmond, J. W.; Fuller, G. G. *Macromolecules* **1993**, *26*, 7182.
(32) Fuller, G. *Optical Rheometry of Complex Fluids*; Oxford University Press: New York, 1995.
(33) Hashimoto, T.; Takebe, T.; Suehiro, S. *Polym. J.* **1986**, *18*, 123.
(34) Mendes, J.; E.; Lindner, P.; Buzier, M.; Boue, F.; Bastide, J. *Phys. Rev. Lett.* **1991**, *66*, 1595.
(35) Onuki, A. *J. Phys. II Fr.* **1992**, *2*, 45.
(36) Zielinski, F.; Buzier, M.; Lartigue, C.; J.; B.; Boué, F. *Prog. Colloid Polym. Sci.* **1992**, *90*, 115.
(37) Matsuzaka, K.; Hashimoto, T. *Rev. Sci. Instrum.* **1999**, *70*, 2387.
(38) Koizumi, S.; Suehiro, S.; Hashimoto, T. Unpublished work.
(39) c^* was calculated using $c^* = 3M_w/4\pi R_g^3 N_A$ with $R_g = b(N_w/6)^{0.5}$, where R_g, N_A, b, and N_w are, respectively, the radius of gyration of a single polymer molecule, Avogadro's number, the statistical segmental length, and the weight-average degree of polymerization.
(40) Saito, S.; Matsuzaka, K.; Hashimoto, T. *Macromolecules* **1999**, *32*, 4879.
(41) The scattering intensity perpendicular to the flow direction at $\omega = 12.27$ rad/s exceeds that parallel to the flow direction in the low-SALS-q region. As shown in the scattering patterns at $\omega = 12.27$ rad/s in Figure 5, there are some artificial scattering along the vertical direction from the beam stopper. This arose from the tiny bubbles that could not be removed when the solution was put into the shear cell and also brought about some upturn of the scattering profile perpendicular to the flow direction in the low-q region.
(42) de Gennes, P. G. *Scaling Concepts in Polymer Physics*; Cornell University Press: Ithaca: NY, 1979.
(43) Nicolai, T.; Brown, W. *Macromolecules* **1996**, *29*, 1698.
(44) Debye, P.; Bueche, A. M. *J. Appl. Phys.* **1949**, *20*, 518.
(45) Debye, P.; Anderson, H. R.; Brumberger, H. *J. Appl. Phys.* **1957**, *28*, 679.
(46) Takebe, T.; Fujioka, K.; Sawaoka, R.; Hashimoto, T. *J. Chem. Phys.* **1990**, *93*, 5271.
(47) Lai, J.; Fuller, G. G. *J. Rheol.* **1995**, *39*, 893.

MA9910336